Causal Discovery from Conditionally Stationary Time Series

Abstract

Causal discovery, i.e., inferring underlying causal relationships from observational data, has been shown to be highly challenging for AI systems. In time-series modeling context, existing causal discovery methods mainly consider constrained scenarios with fully observed variables and/or data from stationary time-series. We develop a causal discovery approach to a wide class of non-stationary time-series that are *conditionally stationary*, where the non-stationary behaviour is modeled as stationarity conditioned on a set of (possibly hidden) state variables whose dynamics may be dependent on the observed sequence. Named State-Dependent Causal Inference (SDCI), our approach is able to recover the underlying causal dependencies, provably with fully-observed states and empirically with hidden states. The latter is confirmed by experiments on both synthetic linear system and spring-connected particle interaction data, where SDCI achieves superior performance over baseline causal discovery methods.

1 INTRODUCTION

Deep learning has achieved profound success in vision and language modelling tasks [Brown et al., 2020, Nichol et al., 2021]. Still, it remains a grand challenge and a prominent research direction to enable deep neural networks to perform causal discovery and reasoning [Yi et al., 2020, Girdhar and Ramanan, 2020, Sauer and Geiger, 2021], which is an inherent mechanism in human cognition [Spelke and Kinzler, 2007]. Specifically for analysing time series data, causal discovery involves identifying the underlying temporal causal structure of the observed sequences. Many existing causal discovery approaches for time series assume stationarity [Granger, 1969, Peters et al., 2017, Löwe et al., 2020, Li et al., 2020, Tank et al., 2021], which is restrictive as sequence data from real-world scenarios are often non-stationary with potential hidden confounders. Recent works introduce a number of different assumptions to tackle causal discovery for non-stationary time series [Zhang et al., 2017, Ghassami et al., 2018, Huang et al., 2019], but in general, causal discovery on non-stationary time series under mild and realistic assumptions is an open problem.

This work aims at addressing this open challenge by proposing a causal discovery algorithm for *condionally stationary time series*, for which the dynamics of the observed system change depend on a set of "state" variables. This assumption holds for many real-world scenarios, e.g., with people who behave differently and take different decisions depending on underlying factors such as mood, previous experience, and the actions of other agents. The causal discovery task for such conditionally stationary time series poses different challenges depending on the observability of the states, which is classified into 4 different scenarios:

1. **Scenario class 1** concerns the simplest case, where the states are observed and their dynamics are independent on other observed time series data (Figure 1a).
2. In **Scenario class 2**, the states are unobserved and directly dependent on observed variables. One example is to consider an agent moving in a room where different behaviors are observed depending on their location. Figure 1b illustrates a similar setting.
3. **Scenario class 3** is more challenging: the state depends on earlier events, and thus cannot be directly inferred from observations. Figure 1c illustrates this regime with particles that change state on wall collision. Also in a football game the action of one player is triggered by an earlier action by another player.
4. Finally, a large share of real-world scenarios (e.g., Figure 1d) are governed by underlying states that are not fully identifiable from the observations over time. Here the states can be unknown confounders to the observed time series, thus the causal discovery task is ill-defined.

Submitted to the 38th Conference on Uncertainty in Artificial Intelligence (UAI 2022). **To be used for reviewing only**.

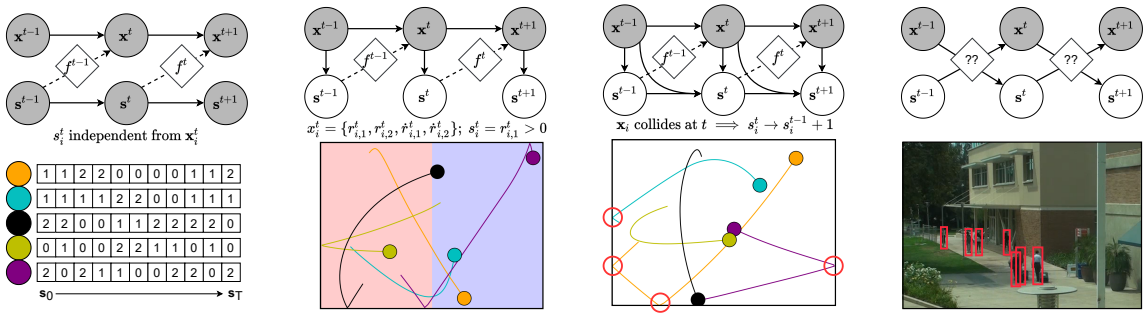

(a) scenario class 1 (b) scenario class 2 (c) scenario class 3 (d) other scenarios

Figure 1: Graphical representations of the data generation processes considered in this work. $\mathbf{x}^t$ represents the observations of a time series sequence, and $\mathbf{s}^t$ denotes the state variables. The state affects the future observations by changing the causal structure (denoted as f^t) for different state values. The representations are examples of (a) scenario class 1, (b) scenario class 2, (c) scenario class 3, and (d) other scenarios (image adapted from Oh et al. [2011]).

Our approach, named State-Dependent Causal Inference (SDCI), is based on discovering the summary graphs *conditioned on states* given observed sequences. It fits a graph neural network based variational auto-encoder [Löwe et al., 2020] to the non-stationary time series data, which enables efficient amortization for causal discovery across multiple observation sequences. We prove identifiability results for cases with fully-observed states; empirically SDCI also applies to cases with hidden states, which is confirmed by experiments on both synthetic linear datasets and spring data (See Figures 1b & 1c), covering scenario classes 1-3. Compared to baselines, SDCI achieves better accuracy in identifying the underlying causal graph structure as well as forecasting future trajectories from historical observations.

2 RELATED WORK

Causal discovery aims to identify causal relationshipsfrom observational data [Glymour et al., 2019]. *Constraint-based* methods rely on conditional independence tests to recover the underlying DAG structure of the data. Representative approaches include the PC algorithm [Spirtes et al., 2000] and Fast Causal Inference (FCI) [Spirtes, 2001], and their extension to time series [Entner and Hoyer, 2010, Runge, 2018]. *Score-based* methods, such as Greedy Equivalence Search (GES) [Chickering, 2002], define and optimize score functions of causal graphs to identify the underlying causal structure. Regarding time series, these methods are reformulated as learning *Dynamic* Bayesian Networks (DBNs) from data [Murphy et al., 2002]. A recent approach in this line is DYNOTEARS [Pamfil et al., 2020]. *Functional causal model-based* methods represent the effect as a function of its direct causes and their independent immeasurable noise [Shimizu et al., 2006, Zhang and Hyvärinen, 2009, Peters et al., 2014, Glymour et al., 2019]. For time series, these approaches fit a dynamic model, which is often constrained in terms of its functional form and connection sparsity in favor of identifiability guarantees [Peters et al., 2013].

Our work is concerned in modelling non-stationary time series using state variables as entities responsible for changing the dynamics along the sequence. Saggioro et al. [2020] uses similar ideas for reconstructing regime-dependent dynamics. Most relevant to ours is Amortized Causal Discovery (ACD) [Löwe et al., 2020], which assumes stationary time series and amortizes summary graph extraction process from samples with different graphs but shared dynamics. Similar ideas are also proposed in Li et al. [2020] for video applications. We extend ACD by allowing the underlying causal structure to vary depending on some state variables. For other related works, Huang et al. [2015] extended Gaussian Process regression for the identification of time-varying functional causal models, Zhang et al. [2017] used kernel embeddings to detect distribution shifts in heterogeneous data. Ghassami et al. [2018] and Huang et al. [2019] estimated the time-varying causal effects. However, the latter two methods are limited by their linear causal model assumptions and fixed causal structures.

3 STATE-DEPENDENT CAUSAL INFERENCE (SDCI)

We introduce SDCI to extract causal graphs from time series data where their dynamics are altered by means of a set of categorical variables, referred to as their states.

3.1 PROBLEM FORMULATION

We consider a dataset $\mathcal{D}$, where each sample $\mathbf{X} \sim \mathcal{D}$ consists of N non-stationary time series $\mathbf{X} = \{\mathbf{x}_1, \ldots, \mathbf{x}_N\}$ of length T. We denote element i at time-step t as $\mathbf{x}_i^t \in \mathbb{R}^d$.

Stationary time series. We assume that the data generation process obeys a structural causal model (SCM) [Pearl, 2009], where all the observed variables $\mathbf{x}_i^t \in \mathcal{V}^{1:T}$ are its vertices, for each time series i at each time-step t, and that there are no instantaneous effects and no hidden confounders. Moreover, same as the definitions of Granger causality [Granger, 1969], we assume that edges of a causal

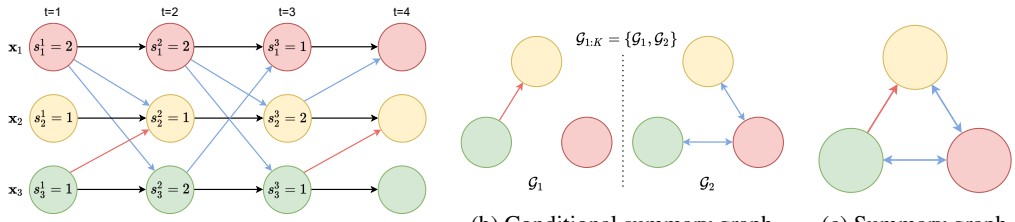

(a) Full time graph (b) Conditional summary graph (c) Summary graph

Figure 2: (a) Full time graph $\mathcal{G}^{1:T}$ of a sample considering our problem setting, (b) conditional summary graph $\mathcal{G}_{1:K}$, and (c) summary graph $\mathcal{G}$ of the corresponding sample. Different colors (red and blue) denote effects caused by different states.

graph cannot go back in time. For the sake of clarity, the underlying causal structure satisfies the first-order Markov property in this work; however, one could directly extend it to the higher order. When considering causality in time series, the corresponding causal graph of a SCM is called *full time graph* [Peters et al., 2017], $\mathcal{G}^{1:T}$. Note that our treatment of stationarity refers to the structure of the causal mechanisms; i.e. edges are invariant in time.

Assumptions similar to the previous ones have been introduced in the past for the analysis of causality considering stationary time series data [Löwe et al., 2020, Li et al., 2020], where the task is to extract the *summary graph*, $\mathcal{G} = \{\mathcal{V}, \mathcal{E}\}$, where $\mathcal{V} = \{\mathbf{x}_1, \dots, \mathbf{x}_N\}$ and an edge from $\mathbf{x}_i$ to $\mathbf{x}_j$ is included in $\mathcal{E}$ if there exists $1 \leq t < t' \leq T$ such that there is an edge from $\mathbf{x}_i^t$ to $\mathbf{x}_j^{t'}$ in the full time graph. Both *full time graph* and *summary graph* are identifiable from observational data as shown by Peters et al. [2013] if the generative process satisfies *Time Series Models with Independent Noise* (TiMINo). We further assume first-order Markov property and an additive noise model (ANM) without instantaneous effects for the generative process:

$$\mathbf{x}_j^t = f_j\left((\mathbf{PA}_j^1)^{t-1}\right) + \boldsymbol{\epsilon}_j^t \tag{1}$$

where $\mathbf{PA}_j^1 \subseteq \mathcal{V}$ denotes the parents of $\mathbf{x}_j$ and $\boldsymbol{\epsilon}_j^t$ denotes independent noise. The direct causes of $\mathbf{x}_j^t$ are $\mathbf{PA}(\mathbf{x}_j^t) = (\mathbf{PA}_j^1)^{t-1} \subset \mathcal{V}^{1:T}$. As here the time series is stationary, we can regard this as first querying the summary graph $\mathcal{G}$ to extract the parents, and then using the correct temporal index $(t-1)$ as a superscript of each parent $(\mathbf{PA}_j^1)$.

Conditionally stationary time series. For non-stationary time series considered in this work, we assume that at each time-step t we have access to state variables $\mathbf{s}^t = \{s_1^t, \dots, s_N^t\}$, where $s_i^t \in \{1, ..., K\}$ controls the causal effects of $\mathbf{x}_i^t$ to future variables $\mathbf{x}_{1:N}^{t+1}$. In other words, when the state s_i^t changes, so do the causal effects for $\mathbf{x}_i^t$. We further assume that the time series is stationary if the states are held constant along the sequence, i.e., $\mathbf{s}^1 = \dots = \mathbf{s}^T$. For the general case where $\mathbf{s}^t$ changes through time, even though the time series is non-stationary, it is *conditionally stationary* given the state variables $\mathbf{S} = \{\mathbf{s}^1, \dots, \mathbf{s}^T\}$.

Figure 2a illustrates the full time graph of a conditionally stationary time series example following our assumptions. In this case a variable affects different sets of future variables depending its state, and the time series is non-stationary as $\mathbf{s}^1 \neq \mathbf{s}^2 \neq \mathbf{s}^3$. Note that the states are not included explicitly in the SCM of the generative process (otherwise the SCM requires additional variables with their own vertices for $\mathbf{S}$). This is a valid simplification since we assume access to the states at all times. Our theoretical results presented below do not apply when considering hidden states, since one must then explicitly model its causal structure in the SCM.

Conditional summary graph. Our goal for causal discovery is to recover the *full time graph*, where for stationary time series this can be achieved by identifying the summary graph under the first-order Markov assumption. However for conditionally stationary time series, the summary graph can be non-informative (probably close to a fully connected graph), due to different causal effects induced by variables in different states. As an example, Figure 2c shows the summary graph extracted from the full time graph of Figure 2a. Being dense, the summary graph as defined for stationary time series is less useful in non-stationary settings. To address this issue, for conditionally stationary time series we define the *conditional summary graph*.

Definition 1 (Conditional summary graph, first-order Markov setting)**.** *Given a full time graph $\mathcal{G}^{1:T}$, its conditional summary graph is a set of K summary graphs, $\mathcal{G}_{1:K} = \{\mathcal{G}_k : 1 \leq k \leq K\}$, where K is the number of possible state values. Each summary graph $\mathcal{G}_k = \{\mathcal{V}, \mathcal{E}_k\}$ has the same vertices $\mathcal{V} = \{\boldsymbol{x}_1, \dots, \boldsymbol{x}_N\}$, and an edge from $\boldsymbol{x}_i$ to $\boldsymbol{x}_j$ is added to $\mathcal{E}_k$ if there exists a time-step $1 \leq t \leq T$ such that $s_i^t = k$ and in $\mathcal{G}^{1:T}$, $\boldsymbol{x}_i^t$ is connected to $\boldsymbol{x}_j^{t+1}$.*

Note that both summary and conditional summary graphs do not include auto-regressive connections $\mathbf{x}_i^t \to \mathbf{x}_i^{t+1}$. Figure 2b shows the conditional summary graph extracted from the full time graph of Figure 2a. For $k = 1$ we have $s_3^1 = 1$ and there is a "red edge" connecting $\mathbf{x}_3^1$ and $\mathbf{x}_2^2$, therefore for $\mathcal{G}_1$ there is a "red edge" in the edge set $\mathcal{E}_1$. Similar reasoning applies for $\mathcal{G}_2$. Compared to the summary graph 2c, the conditional summary graph contains a compact, yet valid representation of the causal structure, and thus being more informative. Although the conditional summary graph can present connections to some related work [Saggioro et al., 2020], ours is more flexible. In other words, we do not restrict the entire time series to be in one of the K states, but allow each variable to be in one of the K different ones.

State-dependent TiMINo. We extend TiMINo to conditionally stationary time series with observed states and

show the identifiability of both full time graph and conditional summary graph. Consider the update on $\mathbf{x}_j^t$ as in Eq. 1. First for non-stationary time series the direct causes of $\mathbf{x}_j^t$, $\mathbf{PA}(\mathbf{x}_j^t)$, are no longer constant in time. However, for conditionally stationary time series satisfying first-order Markov property and our assumptions specified above, $\mathbf{PA}(\mathbf{x}_j^t)$ is determined by the states at the previous time-step $t-1$. Thus we can write $\mathbf{PA}(\mathbf{x}_j^t) = (\mathbf{PA}_j^1|\mathbf{s}^{t-1})^{t-1}$ and the *state-dependent TiMINo* as (with first-order Markov assumption, an ANM model and no instantaneous effect):

$$\mathbf{x}_j^t = f_j^{\mathbf{s}^{t-1}}\left((\mathbf{PA}_j^1|\mathbf{s}^{t-1})^{t-1}\right) + \boldsymbol{\epsilon}_j^t, \quad (2)$$

$$\mathbf{PA}_j^1|\mathbf{s}^{t-1} = \{\mathbf{x}_i : \mathbf{x}_j \in C_i(s_i^{t-1}), 1 \leq i \leq N\}, \quad (3)$$

where $s_i^{t-1} \in \{1, \dots, K\}$ and $C_i(k) \subseteq \mathcal{V}$ denotes the children of variable $\mathbf{x}_i$ when its associated state equals to k. To illustrate, in Figure 2a we have that $\mathbf{PA}(\mathbf{x}_2^2) = \{\mathbf{x}_1^1, \mathbf{x}_2^1, \mathbf{x}_3^1\}$ because $\mathbf{x}_2 \in C_1(s_1^1)$ and $\mathbf{x}_2 \in C_3(s_3^1)$; however $\mathbf{PA}(\mathbf{x}_2^3) = \{\mathbf{x}_1^2, \mathbf{x}_2^2\}$ because now $\mathbf{x}_2 \in C_1(s_1^2)$ but $\mathbf{x}_2 \notin C_3(s_3^2)$.

Identifiability of state-dependent TiMINo. As we assume access to the state variables at all times, the original properties of Markov assumption and causal minimality are maintained, which are satisfied by TiMINo. Consequently, the *conditional summary graph* becomes identifiable by extending the identifiability proof of Peters et al. [2013] to our setting and further assuming that all the states are visited at least once. Notice that failing to observe data corresponding to a particular state of one variable makes it practically impossible to capture the underlying effect of that variable conditioned on the unvisited state. More details for the preservation of causal minimality and Markov condition in the state-dependent TiMINo, the identifiability of both the full time graph and conditional summary graph, and extensions to incorporate other time-lagged or instantaneous effects can be found in Appendix A and B.

State-dependent causal inference. We mainly focus on non-stationary causal graphs which may have different edge-types at different times. Based on our assumptions, the interaction (i.e., edge-type) $\mathbf{x}_i \to \mathbf{x}_j$ can change according to the state of the variable $\mathbf{x}_i$. Following Kipf et al. [2018], Li et al. [2020], Löwe et al. [2020], we consider this edge-type for $\mathbf{x}_i \to \mathbf{x}_j$ at time t as a categorical variable $z_{ij}^t \in \{0, \dots, n_\epsilon - 1\}$ which can represent n_ϵ interaction types between pairs of variables. Specifically we use edge-type 0 to denote "no causal effect" between two variables. Notice that the edge-type differs from the state: the former controls the functional form of the causal effect and the latter allows the variables to affect others differently along time. For example, one can have $\mathbf{x}_i \to \mathbf{x}_j$ whenever $z_{ij}^t \neq 0$, but the functional form of the causal relationship can differ.

The main focus of our method consists on extracting a *conditional summary graph* $\mathcal{G}_{1:K}$ (assuming there exist K states). Previous approaches aiming for this task assume stationary time series data for which $\mathcal{G}_1 = \cdots = \mathcal{G}_K$. For conditionally stationary time series, we extract the k-th summary graph including edge-types, $\tilde{\mathcal{G}}_k = \{\mathcal{V}, \tilde{\mathcal{E}}_k\}$, where $\tilde{\mathcal{E}}_k$ and $\tilde{\mathcal{E}}_{k'}$ can differ for $k \neq k'$. We further define $\tilde{\mathcal{E}}_k = \{w_{ijk} \in \{0, \dots, n_\epsilon - 1\} : \mathbf{x}_i, \mathbf{x}_j \in \mathcal{V}\}$ as the collection of edge types for variable pairs in $\mathcal{V}$. Note here that an edge is visualised in the conditional summary graph visualisation only when $w_{ijk} \neq 0$ (see Figure 2b). Then the edge-type interaction $\mathbf{x}_i \to \mathbf{x}_j$ can be queried at each time-step t as follows:

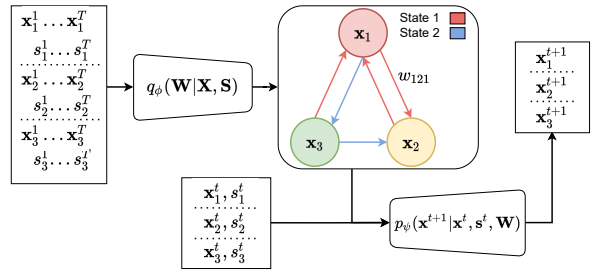

Figure 3: SDCI aims to extract a *conditional summary graph* that describes the edge-type interaction $\mathbf{W} = \{w_{ijk}\}$ for every pair of edges conditioned on the state of the source variable with respect to the interaction.

$$z_{ij}^t = \left(\tilde{\mathcal{E}}_{s_i^t}\right)_{ij}, \quad \left(\tilde{\mathcal{E}}_{s_i^t}\right)_{ij} = w_{ijk} \text{ if } s_i^t = k. \quad (4)$$

Therefore, causal discovery for conditionally stationary time series requires extracting the (unknown) conditional summary graph given observations of $\mathbf{X}$ (and perhaps also $\mathbf{S}$). It not only requires to design a parametrizable function to infer the causal structure, but also to evaluate how this inference fits to the input observations.

3.2 IMPLEMENTATION

We introduce a probabilistic approach which models the distribution of the edge-types $\{z_{ij}^t\}$ given observed data. Following our assumptions for conditionally stationary time series, this task can be solved by learning the distribution of $\mathbf{W} = \{w_{ijk} : 1 \leq i, j \leq N, 1 \leq k \leq K\}$ given data, as after inferring $\mathbf{W}$ one can then query the edge-types z_{ij}^t as in Eq. 4. Inspired by previous approaches [Li et al., 2020, Löwe et al., 2020, Kipf et al., 2018], our implementation is based on a variational auto-encoder (VAE) [Kingma and Welling, 2014] and graph neural networks. We first discuss our approach for the case with fully observed states, then extend the method to the hidden state regime. A diagram of the proposed approach is visualised in Figure 3.

Encoder. Similar to Löwe et al. [2020], we use a factorized q distribution $q_\phi(\mathbf{W}|\mathbf{X}, \mathbf{S}) = \prod_{k=1}^K \prod_{ij} q_\phi(w_{ijk}|\mathbf{X}, \mathbf{S})$. The encoder receives both $\mathbf{X}$ and $\mathbf{S}$ as the input, and extracts an embedding that represents the causal interaction conditioning on the state for every possible edge $\mathbf{x}_i \to \mathbf{x}_j$:

$$\boldsymbol{\phi}_{ij} = f_\phi(\mathbf{X}, \mathbf{S})_{ij} \in \mathbb{R}^{K \times n_\epsilon}, \quad (5)$$

where $f_\phi(\mathbf{X}, \mathbf{S})$ is a neural network that returns outputs $\{\boldsymbol{\phi}_{ij} : 1 \leq i, j \leq N\}$ given the input as $\mathbf{X}$ concatenated with a one-hot representation of the state variable $\mathbf{S}$. The approximate posterior $q_\phi(w_{ijk}|\mathbf{X}, \mathbf{S})$ is calculated as

$$q_\phi(w_{ijk}|\mathbf{X},\mathbf{S}) = \Theta(\boldsymbol{\phi}_{ijk}/\tau) \tag{6}$$

where $\Theta(\cdot)$ denotes a softmax activation with temperature τ. Note here the softmax activation is taken over the k-th row vector $\boldsymbol{\phi}_{ijk} \in \mathbb{R}^{n_\epsilon}$ in $\boldsymbol{\phi}_{ij}$, which is the edge embedding for $\mathbf{x}_i \to \mathbf{x}_j$ at state k. As this returns a categorical distribution for $q_\phi(w_{ijk}|\mathbf{X},\mathbf{S})$, we apply the Gumble-softmax trick [Maddison et al., 2017, Jang et al., 2016] to enable direct differentiation for back-propagation during training.

The construction of $f_\phi(\mathbf{X},\mathbf{S})$ is based on graph neural networks, MLPs and/or CNNs. We experiment with different architecture designs, and in the main text we focus on a particular one named SDCI-Static which uses full-sequence embedding in the message passing procedure. See Appendix D.1 for more details and additional results.

Decoder for X. The decoder for the observations $\mathbf{X}$ given edge-types $\mathbf{W}$ (e.g., sampled as $w_{ijk} \sim q_\phi(w_{ijk}|\mathbf{X},\mathbf{S})$) and the states $\mathbf{S}$ are defined following the first-order Markov assumption (with $\mathbf{x}^0, \mathbf{s}^0$ as dummy variables):

$$p_\psi(\mathbf{X}|\mathbf{W},\mathbf{S}) = \prod_{t=0}^{T-1} p_\psi(\mathbf{x}^{t+1}|\mathbf{x}^t,\mathbf{s}^t,\mathbf{W}), \tag{7}$$

$$p_\psi(\mathbf{x}^{t+1}|\mathbf{x}^t,\mathbf{s}^t,\mathbf{W}) = \prod_{j=1}^{N} \mathcal{N}(\tilde{\mathbf{x}}_j^{t+1}, \sigma^2\mathbb{I}). \tag{8}$$

The mean $\tilde{\mathbf{x}}_j^{t+1}$ is defined as follows. Given sampled edge-types $\mathbf{W} = \{w_{ijk}\}$, the decoder first queries the edge-type for element j at time $t+1$ as $z_{ij}^t = w_{ijk'}$ for $s_i^t = k'$ (also see Eq. 4). Then the information along the predicted edge-type interactions is retrieved as follows [1]

$$\mathbf{h}_{ij}^t = \sum_{e>0} \mathbf{1}_{(z_{ij}^t = e)} f_e(\mathbf{x}_i^t, \mathbf{x}_j^t) \tag{9}$$

where $\{f_e\}_{e=1}^{n_\epsilon - 1}$ is a set of parametrizable functions, one defined for each edge type excluding the no-edge interaction. The interactions are finally integrated to model the dynamics of each variable, where the mean for $\mathbf{x}_j^{t+1}$ is defined as

$$\tilde{\mathbf{x}}_j^{t+1} = \mathbf{x}_j^t + f_p\Big(\sum_{i \neq j} \mathbf{h}_{ij}^t, \mathbf{x}_j^t\Big), \tag{10}$$

where f_p is a neural network that aggregates the information from the previous time-step for prediction.

Training objective. The encoder $q_\phi(\mathbf{W}|\mathbf{X},\mathbf{S})$ and decoder $p_\psi(\mathbf{X}|\mathbf{W},\mathbf{S})$ are trained using a VAE objective:

$$\mathcal{L} = \sum_{t=0}^{T-1} \mathbb{E}_{q_\phi(\mathbf{W}|\mathbf{X},\mathbf{S})}\big[\log p_\psi(\mathbf{x}^{t+1}|\mathbf{x}^t,\mathbf{s}^t,\mathbf{W})\big] - KL\big(q_\phi(\mathbf{W}|\mathbf{X},\mathbf{S})||p(\mathbf{W})\big). \tag{11}$$

We used a factorised prior $p(\mathbf{W}) = \prod_{k=1}^{K}\prod_{ij} p_k(w_{ijk})$ which acts as a regularizer over the inferred edge-type distribution q_ϕ. In our experiments we set this prior to be Uniform$(\{0,\dots,n_\epsilon - 1\})$, although in certain applications it may be useful to use different p_k to encourage different sparsity levels for $\mathcal{G}_k$.

Our method can also be extended to capture the state dynamics and also consider hidden states, despite the latter losing identifiability guarantees due to violations of our assumption. We provide the corresponding details in Appendix C.

4 EXPERIMENTS

We evaluate SDCI on two non-stationary time series synthetic datasets. Our results are compared to Amortized Causal Discovery (ACD) [Löwe et al., 2020], TdFCM Huang et al. [2015], CD-NOD [Zhang et al., 2017], and SAEM [Huang et al., 2019].

4.1 EXPERIMENTS ON LINEAR DATA

We start using linear message passing operations between a number of different time series. Conditioned on the states, the variables $\mathbf{x}_i^t, \mathbf{x}_j^{t+1} \in \mathbb{R}$ are connected by an edge of n_ϵ different types. Each edge-type is captured by the linear coefficients $\{\beta_k \in \mathbb{R}\}_{k=0}^{n_\epsilon - 1}$ with the convention that $\beta_0 = 0$ (as edge-type 0 represents no connection). Notice that the effect of $\mathbf{x}_i^t$ on $\mathbf{x}_j^{t+1}$ changes during time according to the state value s_i^t and the underlying conditional summary graph $\mathcal{G}_{1:K}$. Details of the data generation, training specifications, and additional experiments can be found in Appendices F.1, D.2, and G.1 respectively.

Scenario class 2. We consider simulations following scenario class 2 (see Figure 1b), where the states are hidden from the input data (only $\mathbf{X}$ is given). This enables comparisons with TdFCM, CD-NOS and SAEM which perform causal discovery based on $\mathbf{X}$ only. As these two baseline methods consider constant causal connections (i.e., a single summary graph) model the non-stationary behaviour differently, for a fair comparison we evaluate the identification accuracy of the summary graph in a way such that it only considers the existence of an edge rather than capturing the edge type. We simulate $N = 3$ variables with 2 edge-types (2-EDGE), 3 edge-types with constant summary graphs (3-EDGE CONST) and 3 edge-types with no constraints on the conditional summary graph (3-EDGE FREE).

We report the (conditional) summary graph identification accuracies in Table 1. It is clear that SDCI performs the best in extracting both the summary graph and conditional summary graph of the underlying data distribution. Since ACD relies on stationary time series, it achieves comparable results when considering a constant causal graph. On the other hand, TdFCM, CD-NOD and SAEM perform significantly worse, as they are designed for non-stationary time series with distribution shifts and smooth time-varying coefficients, which are not suited for time series data with discrete changes in its dynamics. Furthermore, as compared with TdFCM, CD-NOD and SAEM which conduct causal

[1] In training, $\mathbf{1}_{(z_{ij}^t = e)}$ is replaced by the e-th dimension of $w_{ijk'}$ which is sampled from q_ϕ with Gumbel-softmax relaxation.

Table 1: Summary graph (SG) and conditional summary graph (CSG) accuracy for linear data in scenario class 2.

METHOD	SG ACCURACY		
	2-EDGE	3-EDGE	
		CONST	FREE
TDFCM (T=100)	65.17 ± 2.65	63.67 ± 1.61	63.50 ± 1.62
CD-NOD (T=100)	39.33 ± 2.59	35.25 ± 2.51	28.58 ± 2.66
SAEM (T=100)	47.75 ± 3.67	39.04 ± 2.38	51.44 ± 3.81
TDFCM (T=1000)	68.25 ± 2.29	61.17 ± 2.28	62.00 ± 2.14
CD-NOD (T=1000)	50.08 ± 2.59	42.08 ± 2.17	41.58 ± 2.02
SAEM (T=1000)	47.38 ± 4.10	25.93 ± 2.82	28.49 ± 3.28
ACD (T=50)	60.45 ± 1.60	87.00 ± 2.56	49.25 ± 3.05
SDCI-STATIC (T=50)	97.08 ± 1.05	90.17 ± 2.22	64.00 ± 2.93
	CSG ACCURACY		
	2-EDGE	3-EDGE	
		CONST	FREE
SDCI-STATIC (T=50)	98.08 ± 0.64	76.04 ± 2.05	65.45 ± 1.99

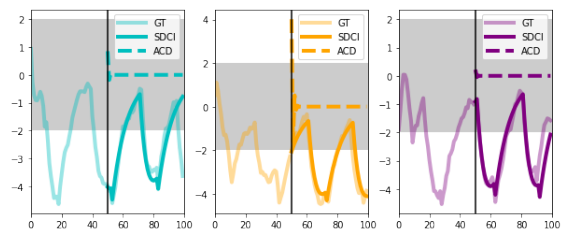

Figure 4: Time series forecasting of SDCI (solid line) and ACD (dashed line) for 50 time-steps after causal inference along with the ground-truth (GT, transparent line). The background represents the state value.

discovery on each multivariate time series separately, both ACD and SDCI benefit from amortized causal graph inference which utilises shared information across different multivariate time series.

For the 2 edge-types setting, we visualise an example time series forecasting result of SDCI and ACD given $T = 50$ observed time-steps in Figure 4, and the associated causal graph identification results in Figure 5. In this particular case, SDCI correctly extracts the conditional summary graph, agreeing with the high CSG accuracy reported in Table 1. In contrast, ACD extracts a single causal graph (which is incorrect), and the forecasts move to 0 rapidly. Close inspection shows that ACD estimates $\alpha < 1$, which in this case without external effects or cycles in the summary graph, it provokes all elements dropping to 0 eventually.

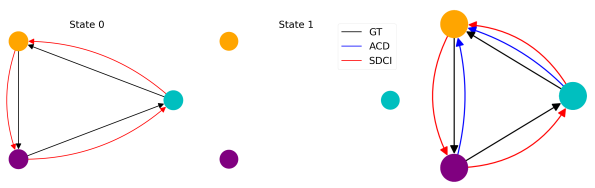

(a) Conditional summary graph (b) summary graph

Figure 5: (a) CSG and (b) SG extracted by SDCI (red) and ACD (blue), along with the ground-truth (black).

Table 2: Test CSG accuracy (in %) and test MSE using spring data with different states for SDCI-STATIC.

K	CSG ACCURACY	TEST MSE
1	99.67 ± 0.13	$7.88 \cdot 10^{-5} \pm 4.64 \cdot 10^{-4}$
2	97.11 ± 0.08	$4.02 \cdot 10^{-2} \pm 1.96 \cdot 10^{-4}$
3	95.79 ± 0.09	$2.33 \cdot 10^{-2} \pm 1.64 \cdot 10^{-4}$
5	80.34 ± 0.10	$6.57 \cdot 10^{-2} \pm 3.23 \cdot 10^{-4}$
8	74.87 ± 0.08	$3.02 \cdot 10^{-2} \pm 1.63 \cdot 10^{-4}$

4.2 EXPERIMENTS ON SPRING DATA

We evaluate our method on the synthetic *spring data* adapted from Kipf et al. [2018], Löwe et al. [2020], which consists of particles connected by springs with directed impact - meaning that e.g. particle i could affect particle j with a force through a connecting spring, but leaving particle i unaffected by this spring force. We consider 2 edge-types (presence/absence of directed spring) and scenario class 1 as presented in Section 1. Details of data generation, model hyper-parameters, and results with other scenario classes can be found in Appendices F.2, D.2 and G.2 respectively.

Scenario class 1. In this experiment the states are known and their dynamics are independent from the observations. For the ground truth dynamics, the state transitions incrementally into the next one every 10 time-steps. Table 2 shows the corresponding results, where we experiment with datasets generated with different number of states $K = 1, 2, 3, 5, 8$. Note that when $K = 1$ the generated time series is stationary, and SDCI's performance matches the results of ACD reported in Löwe et al. [2020]. Although performance drops as K increases, SDCI-Static is able to maintain reasonable CSG accuracy , e.g., 74.87% for $K = 8$.

5 CONCLUSIONS

We have extended the causal discovery task to a class of non-stationary time series named conditionally stationary time series. Key to our development is the state-dependent TiMINo as an extension of [Peters et al., 2013] to conditionally stationary time series, and its identifiability under observed states. We have developed SDCI for amortized causal discovery utilizing the conditional summary graph, and experiments on both synthetic linear and spring data under different scenario classes show better performance in extracting the underlying causal graph and forecasting.

A number of research directions are to be explored in the future. For theoretical studies, identifiability for hidden states can be derived with additional assumptions. For practical applications, SDCI can be applied to time series with states as auxiliary variables for (possibly) indicating non-stationarity regimes. It could also be extended to videos where e.g. the interacting objects are partially and noisily observed as semantically segmented regions. This would enable efficient and effective use of neural networks for causal reasoning in challenging real-world scenarios.

References

Tom Brown, Benjamin Mann, Nick Ryder, Melanie Subbiah, Jared D Kaplan, Prafulla Dhariwal, Arvind Neelakantan, Pranav Shyam, Girish Sastry, Amanda Askell, et al. Language models are few-shot learners. *Advances in neural information processing systems*, 33:1877–1901, 2020.

David Maxwell Chickering. Optimal structure identification with greedy search. *Journal of machine learning research*, 3(Nov):507–554, 2002.

Djork-Arné Clevert, Thomas Unterthiner, and Sepp Hochreiter. Fast and accurate deep network learning by exponential linear units (elus). In Yoshua Bengio and Yann LeCun, editors, *4th International Conference on Learning Representations, ICLR 2016, San Juan, Puerto Rico, May 2-4, 2016, Conference Track Proceedings*, 2016.

Doris Entner and Patrik O Hoyer. On causal discovery from time series data using fci. *Probabilistic graphical models*, pages 121–128, 2010.

Tomas Geffner, Javier Antoran, Adam Foster, Wenbo Gong, Chao Ma, Emre Kiciman, Amit Sharma, Angus Lamb, Martin Kukla, Nick Pawlowski, et al. Deep end-to-end causal inference. *arXiv preprint arXiv:2202.02195*, 2022.

AmirEmad Ghassami, Negar Kiyavash, Biwei Huang, and Kun Zhang. Multi-domain causal structure learning in linear systems. *Advances in neural information processing systems*, 31, 2018.

Rohit Girdhar and Deva Ramanan. CATER: A diagnostic dataset for Compositional Actions and TEmporal Reasoning. In *ICLR*, 2020.

Clark Glymour, Kun Zhang, and Peter Spirtes. Review of causal discovery methods based on graphical models. *Frontiers in genetics*, 10:524, 2019.

Mingming Gong, Kun Zhang, Bernhard Schoelkopf, Dacheng Tao, and Philipp Geiger. Discovering temporal causal relations from subsampled data. In *International Conference on Machine Learning*, pages 1898–1906. PMLR, 2015.

Clive WJ Granger. Investigating causal relations by econometric models and cross-spectral methods. *Econometrica: journal of the Econometric Society*, pages 424–438, 1969.

Biwei Huang, Kun Zhang, and Bernhard Schölkopf. Identification of time-dependent causal model: A gaussian process treatment. In *Twenty-Fourth international joint conference on artificial intelligence*, 2015.

Biwei Huang, Kun Zhang, Mingming Gong, and Clark Glymour. Causal discovery and forecasting in nonstationary environments with state-space models. In *International Conference on Machine Learning*, pages 2901–2910. PMLR, 2019.

Eric Jang, Shixiang Gu, and Ben Poole. Categorical reparameterization with gumbel-softmax. *arXiv preprint arXiv:1611.01144*, 2016.

Diederik P. Kingma and Jimmy Ba. Adam: A method for stochastic optimization. In Yoshua Bengio and Yann LeCun, editors, *3rd International Conference on Learning Representations, ICLR 2015, San Diego, CA, USA, May 7-9, 2015, Conference Track Proceedings*, 2015.

Diederik P. Kingma and Max Welling. Auto-Encoding Variational Bayes. In *2nd International Conference on Learning Representations, ICLR 2014, Banff, AB, Canada, April 14-16, 2014, Conference Track Proceedings*, 2014.

Thomas Kipf, Ethan Fetaya, Kuan-Chieh Wang, Max Welling, and Richard Zemel. Neural relational inference for interacting systems. In *International Conference on Machine Learning*, pages 2688–2697. PMLR, 2018.

Yunzhu Li, Antonio Torralba, Anima Anandkumar, Dieter Fox, and Animesh Garg. Causal discovery in physical systems from videos. In H. Larochelle, M. Ranzato, R. Hadsell, M. F. Balcan, and H. Lin, editors, *Advances in Neural Information Processing Systems*, volume 33, pages 9180–9192. Curran Associates, Inc., 2020.

Zhouhan Lin, Minwei Feng, Cícero Nogueira dos Santos, Mo Yu, Bing Xiang, Bowen Zhou, and Yoshua Bengio. A structured self-attentive sentence embedding. In *5th International Conference on Learning Representations, ICLR 2017, Toulon, France, April 24-26, 2017, Conference Track Proceedings*, 2017.

Sindy Löwe, David Madras, Richard S. Zemel, and Max Welling. Amortized causal discovery: Learning to infer causal graphs from time-series data. *ArXiv*, abs/2006.10833, 2020.

Chris J. Maddison, Andriy Mnih, and Yee Whye Teh. The concrete distribution: A continuous relaxation of discrete random variables. In *5th International Conference on Learning Representations, ICLR 2017, Toulon, France, April 24-26, 2017, Conference Track Proceedings*, 2017.

Kevin P Murphy et al. Dynamic bayesian networks. *Probabilistic Graphical Models, M. Jordan*, 7:431, 2002.

Alex Nichol, Prafulla Dhariwal, Aditya Ramesh, Pranav Shyam, Pamela Mishkin, Bob McGrew, Ilya Sutskever, and Mark Chen. Glide: Towards photorealistic image generation and editing with text-guided diffusion models. *arXiv preprint arXiv:2112.10741*, 2021.

Sangmin Oh, Anthony Hoogs, Amitha Perera, Naresh Cuntoor, Chia-Chih Chen, Jong Taek Lee, Saurajit Mukherjee, JK Aggarwal, Hyungtae Lee, Larry Davis, et al. A large-scale benchmark dataset for event recognition in surveillance video. In *CVPR 2011*, pages 3153–3160. IEEE, 2011.

Roxana Pamfil, Nisara Sriwattanaworachai, Shaan Desai, Philip Pilgerstorfer, Konstantinos Georgatzis, Paul Beaumont, and Bryon Aragam. Dynotears: Structure learning from time-series data. In *International Conference on Artificial Intelligence and Statistics*, pages 1595–1605. PMLR, 2020.

Adam Paszke, Sam Gross, Francisco Massa, Adam Lerer, James Bradbury, Gregory Chanan, Trevor Killeen, Zeming Lin, Natalia Gimelshein, Luca Antiga, Alban Desmaison, Andreas Kopf, Edward Yang, Zachary DeVito, Martin Raison, Alykhan Tejani, Sasank Chilamkurthy, Benoit Steiner, Lu Fang, Junjie Bai, and Soumith Chintala. Pytorch: An imperative style, high-performance deep learning library. In *Advances in Neural Information Processing Systems 32*, pages 8024–8035. Curran Associates, Inc., 2019.

Judea Pearl. *Causality*. Cambridge university press, 2009.

Jonas Peters, Joris M. Mooij, Dominik Janzing, and Bernhard Schölkopf. Identifiability of causal graphs using functional models. In Fabio G. Cozman and Avi Pfeffer, editors, *Proceedings of the 27th Annual Conference on Uncertainty in Artificial Intelligence (UAI-11)*, pages 589–598. AUAI Press, 2011.

Jonas Peters, Dominik Janzing, and Bernhard Schölkopf. Causal inference on time series using restricted structural equation models. *Advances in Neural Information Processing Systems*, 26, 2013.

Jonas Peters, Joris M. Mooij, Dominik Janzing, and Bernhard Schölkopf. Causal discovery with continuous additive noise models. *Journal of Machine Learning Research*, 15(58):2009–2053, 2014.

Jonas Peters, Dominik Janzing, and Bernhard Schölkopf. *Elements of causal inference: foundations and learning algorithms*. The MIT Press, 2017.

Jakob Runge. Causal network reconstruction from time series: From theoretical assumptions to practical estimation. *Chaos: An Interdisciplinary Journal of Nonlinear Science*, 28(7):075310, 2018.

Elena Saggioro, Jana de Wiljes, Marlene Kretschmer, and Jakob Runge. Reconstructing regime-dependent causal relationships from observational time series. *Chaos: An Interdisciplinary Journal of Nonlinear Science*, 30(11): 113115, 2020.

Axel Sauer and Andreas Geiger. Counterfactual generative networks. In *International Conference on Learning Representations*, 2021.

Shohei Shimizu, Patrik O Hoyer, Aapo Hyvärinen, Antti Kerminen, and Michael Jordan. A linear non-gaussian acyclic model for causal discovery. *Journal of Machine Learning Research*, 7(10), 2006.

Christopher A Sims. Macroeconomics and reality. *Econometrica: journal of the Econometric Society*, pages 1–48, 1980.

Elizabeth S Spelke and Katherine D Kinzler. Core knowledge. *Developmental science*, 10(1):89–96, 2007.

Peter Spirtes. An anytime algorithm for causal inference. In *AISTATS*, 2001.

Peter Spirtes, Clark N Glymour, Richard Scheines, and David Heckerman. *Causation, prediction, and search*. MIT press, 2000.

Alex Tank, Ian Covert, Nicholas Foti, Ali Shojaie, and Emily B Fox. Neural granger causality. *IEEE Transactions on Pattern Analysis and Machine Intelligence*, pages 1–1, 2021. doi: 10.1109/TPAMI.2021.3065601.

Kexin Yi, Chuang Gan, Yunzhu Li, Pushmeet Kohli, Jiajun Wu, Antonio Torralba, and Joshua B. Tenenbaum. CLEVRER: collision events for video representation and reasoning. In *ICLR*, 2020.

Kun Zhang and Aapo Hyvärinen. On the identifiability of the post-nonlinear causal model. In *Proceedings of the Twenty-Fifth Conference on Uncertainty in Artificial Intelligence*, UAI '09, page 647–655, Arlington, Virginia, USA, 2009. AUAI Press. ISBN 9780974903958.

Kun Zhang, Zhikun Wang, Jiji Zhang, and Bernhard Schölkopf. On estimation of functional causal models: general results and application to the post-nonlinear causal model. *ACM Transactions on Intelligent Systems and Technology (TIST)*, 7(2):1–22, 2015.

Kun Zhang, Biwei Huang, Jiji Zhang, Clark Glymour, and Bernhard Schölkopf. Causal discovery from nonstationary/heterogeneous data: Skeleton estimation and orientation determination. In *IJCAI: Proceedings of the Conference*, volume 2017, page 1347. NIH Public Access, 2017.

A PROOFS

This section presents the detailed proofs for the theoretical results of our paper. Again we note here that the results only apply when the states **S** are fully observed. Our theory extend on the theoretical results presented in Peters et al. [2013] and Peters et al. [2017], which are presented first before our proofs.

Proposition 1 (Prop. 6.36 in Peters et al. [2017])**.** *Causal minimality is satisfied if and only if* $\forall \boldsymbol{x}_j, \forall \boldsymbol{y} \in \boldsymbol{PA}(\boldsymbol{x}_j)$ *we have that* $\boldsymbol{x}_j \not\perp\!\!\!\perp \boldsymbol{y} | \boldsymbol{PA}(\boldsymbol{x}_j) \backslash \{\boldsymbol{y}\}$

Proposition 2 (Prop. 7.4 in Peters et al. [2017])**.** *Consider a distribution given by the following additive noise model*

$$\boldsymbol{x}_j = f_j(\boldsymbol{PA}(\boldsymbol{x}_j)) + \boldsymbol{\epsilon}_j, \quad j = 1, \ldots, N \tag{12}$$

if the functions f_j *are not constant in any of their arguments, then the joint distribution satisfies causal minimality with respect to the corresponding graph.*

Recall from the main text that *state-dependent TiMINo* is defined as (with first-order Markov assumption, additive noise model, and no instantaneous effect):

$$\mathbf{x}_j^t = f_j^{\mathbf{s}^{t-1}}\left((\mathbf{PA}_j^1|\mathbf{s}^{t-1})^{t-1}\right) + \boldsymbol{\epsilon}_j^t, \tag{13}$$

$$\mathbf{PA}_j^1|\mathbf{s}^{t-1} = \{\mathbf{x}_i : \mathbf{x}_j \in C_i(s_i^{t-1}), 1 \leq i \leq N\}. \tag{14}$$

Below we derive the identifiability results for state-dependent TiMINo given fully observed states **S**.

A.1 STATE-DEPENDENT TIMINO PRESERVES MARKOV CONDITION

We show that the state-dependent TiMINo is Markov.

Lemma 1. *Given the states* $\boldsymbol{S}$*, if* $\boldsymbol{X}$ *is generated by a state-dependent TiMINo, then each variable is conditionally independent of each non-descendants given its parents.*

Proof. As the states **S** are given, we can retrieve the direct causes of $\mathbf{x}_j^t$:

$$P := \mathbf{PA}(\mathbf{x}_j^t) = \{\mathbf{x}_i^{t-1} : \mathbf{x}_j \in C_i(s_i^{t-1}), 1 \leq i \leq N\},$$

and use state-dependent TiMINo to compute $\mathbf{x}_j^t$ given its parents:

$$\mathbf{x}_j^t|_{P=p} = f_j^{\mathbf{s}^{t-1}}(p) + \boldsymbol{\epsilon}_j^t.$$

Given its parents P, variable $\mathbf{x}_j^t$ is therefore independent of its non-descendants. □

A.2 STATE-DEPENDENT TIMINO PRESERVES CAUSAL MINIMALITY

We show that the state-dependent TiMINo model satisfies causal minimality given observed states.

Lemma 2. *Assume all the functions* f_j *in a state-dependent TiMINo are not constant in any of their arguments. Then causal minimality is preserved given observed states.*

Proof. Again as the states **S** are observed, then for any $\mathbf{x}_j^t$ the direct causes of it can be retrieved by:

$$P := \mathbf{PA}(\mathbf{x}_j^t) = \{\mathbf{x}_i^{t-1} : \mathbf{x}_j \in C_i(s_i^{t-1}), 1 \leq i \leq N\}.$$

Assume causal minimality is not satisfied, then following Proposition 1, there exists $\mathbf{x}_j^t$ and $\mathbf{x}_i^{t-1} \in P$ such that

$$\mathbf{x}_j^t \perp\!\!\!\perp \mathbf{x}_i^{t-1} | P \backslash \{\mathbf{x}_i^{t-1}\}$$

Denote $P \backslash \{\mathbf{x}_i^{t-1}\}$ as P_A. Then, if $\mathbb{E}[\boldsymbol{\epsilon}_j^t] = 0$, there exists a function $c(\cdot)$ such that

$$\mathbb{E}\left[\mathbf{x}_j^t\right] = f_j^{\mathbf{s}^{t-1}}\left(P_A, \mathbf{x}_i^{t-1}\right) = c(P_A), \quad \forall \mathbf{x}_i^{t-1}.$$

This implies that $f_j^{\mathbf{s}^{t-1}}$ is constant with respect to $\mathbf{x}_i^{t-1}$. It contradicts with the assumption that $f_j^{\mathbf{s}^{t-1}}$ is not constant in any of its arguments. Therefore, causal minimality in state-dependent TiMINo is preserved given observed states. □

A.3 IDENTIFIABILITY IN STATE-DEPENDENT TIMINO

Using the Markov and causal minimality results, we derived the following identifiability result for state-dependent TiMINo, and the proof is inspired by Peters et al. [2013].

Theorem 1. *Consider the state-dependent TiMINo, where only first-order Markov interactions are present, and there is no instantaneous effects. Then the full time graph* $\mathcal{G}^{1:T}$ *is identifiable from the distribution of data given states.*

Proof. Conditioned on **S**, assume that $\mathbf{x}_t$ can be computed from two state-dependent TiMINo with two different full time graphs, $\mathcal{G}_1^{1:T}$ and $\mathcal{G}_2^{1:T}$. Suppose there is an edge $\mathbf{x}_i^{t-1} \rightarrow \mathbf{x}_j^t$ which is in $\mathcal{G}_1^{1:T}$, but not in $\mathcal{G}_2^{1:T}$.

1. From $\mathcal{G}_2^{1:T}$ and the Markov condition (Lemma 1), we have $\mathbf{x}_j^t \perp\!\!\!\perp \mathbf{x}_i^{t-1} | \{\mathbf{x}_k^{t-1}, 1 \leq k \leq N, k \neq i\}$.
2. From $\mathcal{G}_1^{1:T}$ and causal minimality (Lemma 2), we have $\mathbf{x}_j^t \not\perp\!\!\!\perp \mathbf{x}_i^{t-1} | \{\mathbf{x}_k^{t-1}, 1 \leq k \leq N, k \neq i\}$.

Since we have a contradiction, the full time graphs $\mathcal{G}_1^{1:T}$ and $\mathcal{G}_2^{1:T}$ must be equal. Therefore, the full time graph is identifiable from the distribution of data given states. □

Given the identifiability results, in theory, we can estimate the state-dependent TiMiNo in Eq. 2 with maximum likelihood [Zhang et al., 2015]. In our implementation, we train the model with the modified VAE objective 19. The empirical results show that it infers causal structures correctly; however, it is nontrivial to prove that the identifiability holds with the modified VAE objective, which has been discussed in [Geffner et al., 2022] as well and will be our future work.

A.4 IDENTIFIABILITY OF CONDITIONAL SUMMARY GRAPH

Assuming the full time graph has been extracted successfully, one can deduce the structure of the conditional summary graph by observing the edges of pairs of variables conditioned on the state variable which is the cause of the interaction. In particular, the precise mathematical statement for this identifiability result is as follows, assuming that all the states of each element have been visited at least once in order to condition on each possible state.

Corollary 1. *Consider the state-dependent TiMINo, where only first-order Markov interactions are present, and there is no instantaneous effects. Then the conditional summary graph $\mathcal{G}_{1:K}$ is identifiable given the states **S**, if for any $1 \leq i \leq N$ and any $1 \leq k \leq K$ there exists $1 \leq t \leq T$ such that $s_i^t = k$.*

Proof. Notice that $\mathcal{G}_k = \{\mathcal{V}, \mathcal{E}_k\}$ with $\mathcal{V} = \{\mathbf{x}_1, \dots, \mathbf{x}_N\}$, therefore identifying $\mathcal{G}_k$ is equivalent to identifying the edge set $\mathcal{E}_k$. From the assumptions, the full time graph $\mathcal{G}^{1:T}$ is identifiable (Theorem 1). Then for each variable $\mathbf{x}_j^{t+1}$ we can retrieve from $\mathcal{G}^{1:T}$ the parents $\mathbf{PA}(\mathbf{x}_j^{t+1})$. Then for each $\mathbf{x}_i^t \in \mathbf{PA}(\mathbf{x}_j^{t+1})$, we can query its state s_i^t and add an edge $\mathbf{x}_i \to \mathbf{x}_j$ to the edge set $\mathcal{E}_k$ if $s_i^t = k$. Now for any i, k consider the i-th node in the k-th summary graph $\mathcal{G}_k$, since we assume that there exists $1 \leq t \leq T$ such that $s_i^t = k$, this makes sure that the edges coming out of node $\mathbf{x}_i$ at state k are added to $\mathcal{E}_k$. Therefore this procedure captures all possible edge interactions, and $\mathcal{G}_{1:K}$ is identifiable given identifiability of $\mathcal{G}^{1:T}$. □

Notice that the assumption on each variable visiting all possible states is required if one aims to obtain the full structure of the conditional summary graph. Otherwise, if the state k of a variable $\mathbf{x}_i$ is not visited, this leaves the outgoing edges of the i-th node in $\mathcal{G}_k$ undetermined, since there is no information to extract from the full time graph.

B IDENTIFIABILITY EXTENSIONS FOR STATE-DEPENDENT TIMINO

The first-order Markov assumption makes our definitions and identifiability analysis simpler. However, we argue this can still be very useful because (i) it usually suffices to describe particle trajectories (position, velocity, acceleration, etc), (ii) it allows us to present the conditional summary graph as a compact representation of the causal structure, and (iii) we present a method (SDCI) which leverages this assumption for efficient causal discovery. One could easily extend our identifiability results and definitions to higher order time-lagged effects. Incorporating contemporaneous effects is also possible, but requires further assumptions to consider an *identifiable functional model class* (IFMOC) [Peters et al., 2011] (e.g. linear $f_j^{\mathbf{s}^{t-1}}$ with non-Gaussian disturbances).

C EXTENSIONS OF SDCI

C.1 STATE DEPENDENT ON OBJECT DYNAMICS

Although we assume access to the states at all times and thus we require no supervision upon **S**, we might find practical to consider the setting where the state is in fact dependent on **X**. Therefore, we extend our approach to model the temporal dynamics of **S** by defining the joint distribution $p(\mathbf{X}, \mathbf{S}|\mathbf{W})$ as follows, again following the first-order Markov assumption:

$$p_\psi(\mathbf{X}, \mathbf{S}|\mathbf{W}) = \prod_{t=0}^{T-1} p_\psi(\mathbf{x}^{t+1}, \mathbf{s}^{t+1}|\mathbf{x}^t, \mathbf{s}^t, \mathbf{W}) \tag{15}$$
$$= \prod_{t=0}^{T-1} p_\psi(\mathbf{x}^{t+1}|\mathbf{x}^t, \mathbf{s}^t, \mathbf{W}) p_\psi(\mathbf{s}^{t+1}|\mathbf{x}^t, \mathbf{s}^t, \mathbf{W}),$$

$$p_\psi(\mathbf{s}^{t+1}|\mathbf{x}^t, \mathbf{s}^t, \mathbf{W}) = \prod_{j=1}^{N} p_\psi(s_j^{t+1}|\mathbf{x}^t, \mathbf{s}^t, \mathbf{W}). \tag{16}$$

The distribution $p_\psi(\mathbf{x}^{t+1}|\mathbf{x}^t, \mathbf{s}^t, \mathbf{W})$ is defined as above. For the variable s_j^{t+1}, we use a categorical distribution

$$p_\psi(s_j^{t+1}|\mathbf{x}^t, \mathbf{s}^t, \mathbf{W}) = \Theta(\tilde{s}_j^{t+1}) \tag{17}$$

where the logit $\tilde{s}_j^{t+1} \in \mathbb{R}^{n_\epsilon}$ is computed as

$$\tilde{s}_j^{t+1} = f_s\Big(\sum_{i \neq j} \mathbf{h}_{ij}^t, \mathbf{x}_j^t, s_j^t\Big) \tag{18}$$

with f_s as a neural network that combines information from previous observation, states and the predicted edge-type interactions to predict the next state.

Objective (with S observed). The encoder $q_\phi(\mathbf{W}|\mathbf{X}, \mathbf{S})$ and the decoder & state dynamic model $p_\psi(\mathbf{X}, \mathbf{S}|\mathbf{W})$ are trained using a modified VAE objective:

$$\mathcal{L} = \sum_{t=0}^{T-1} \{\mathbb{E}_{q_\phi(\mathbf{W}|\mathbf{X},\mathbf{S})}\big[\log p_\psi(\mathbf{x}^{t+1}|\mathbf{x}^t, \mathbf{s}^t, \mathbf{W})\big] + \lambda \mathbb{E}_{q_\phi(\mathbf{W}|\mathbf{X},\mathbf{S})}\big[\log p_\psi(\mathbf{s}^{t+1}|\mathbf{x}^t, \mathbf{s}^t, \mathbf{W})\big]\} - KL\big(q_\phi(\mathbf{W}|\mathbf{X}, \mathbf{S})||p(\mathbf{W})\big) \tag{19}$$

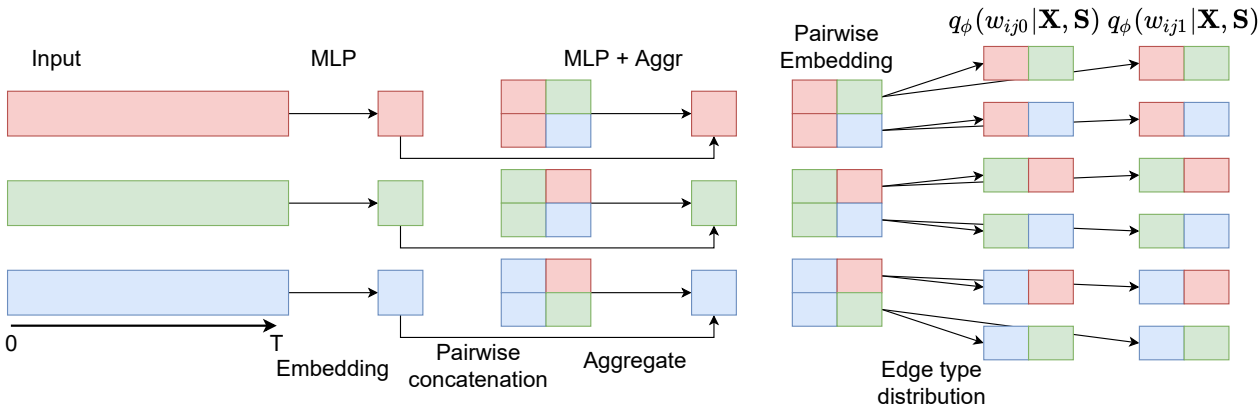

Figure 6: Illustration of the implementation of the SDCI-Static encoder which is adapted from ACD [Löwe et al., 2020] and allow for conditioning on states. In the example, we consider 2 states.

where we use λ to balance the accuracy in learning the decoder for $\mathbf{X}$ and the state dynamics. Here we used a factorised prior $p(\mathbf{W}) = \prod_{k=1}^{K} \prod_{ij} p_k(w_{ijk})$ which acts as a regularizer over the inferred edge-type distribution q. In our experiments we set this prior to be Uniform($\{0, \dots, n_\epsilon - 1\}$), although in certain applications it may be useful to use different p_k to encourage different sparsity levels for $\mathcal{G}_k$.

C.2 HIDDEN STATE REGIME

Often in practice only observations of $\mathbf{X}$ are available, i.e., the states $\mathbf{S}$ are hidden variables. In this case we make a factorised approximation $q_\phi(\mathbf{W}, \mathbf{S}|\mathbf{X}) = q_\phi(\mathbf{W}|\mathbf{X}) q_\phi(\mathbf{S}|\mathbf{X})$, where $q_\phi(\mathbf{W}|\mathbf{X})$ is defined in a similar way as the state fully-observed case (see above) except for using network $f_\phi(\mathbf{X})$ for the softmax logits. For the states, we consider $q_\phi(\mathbf{S}|\mathbf{X}) = \prod_{t=1}^{T} \prod_{i=1}^{N} q_\phi(s_i^t|\mathbf{x}_i^t)$, with each $q_\phi(s_i^t|\mathbf{x}_i^t)$ defined as

$$q_\phi(s_i^t|\mathbf{x}_i^t) = \Theta(\hat{s}_i^t/\gamma), \quad \hat{s}_i^t = \hat{f}_s(\mathbf{x}_i^t), \tag{20}$$

with $\gamma < 1$ as a temperature factor and $\hat{f}_s$ as a neural network. For the decoding process given $\mathbf{W} \sim q_\phi(\mathbf{W}|\mathbf{X})$, we do not explicitly perform the edge query step for z_{ij}^t as it needs samples s_{ij}^t from $q_\phi(\mathbf{S}|\mathbf{X})$. Instead we directly compute the $\mathbf{h}_{ij}^t$ information for the predicted interaction $\mathbf{x}_i \to \mathbf{x}_j$ at time t by marginalising out s_i^t:

$$\mathbf{h}_{ij}^t = \sum_{k=1}^{K} q_\phi(s_i^t = k|\mathbf{x}_i^t) \sum_{e>0} \mathbf{1}_{(w_{ijk}=e)} f_e(\mathbf{x}_i^t, \mathbf{x}_j^t), \tag{21}$$

and we apply similar Gumbel-softmax tricks as in the fully-observed state case to replace $\mathbf{1}_{(w_{ijk}=e)}$ during training. The VAE training objective in this case is similar to Eq. 19 except that the expectations of the log-likelihood terms are taken under distribution $q_\phi(\mathbf{W}, \mathbf{S}|\mathbf{X})$, and the KL regulariser is replaced by $KL\big(q_\phi(\mathbf{W}|\mathbf{X})||p(\mathbf{W})\big)$. We do not include the entropy $\mathbb{H}[q_\phi(\mathbf{S}|\mathbf{X})]$ in the objective as one would have done in sequential VAEs: as $\mathbf{S}$ are discrete, the entropy is always non-negative, meaning that removing it still results in a valid variational lower-bound.

Note that in this hidden state regime the previous theoretical guarantees on identifiability no longer hold due to violations of our assumptions. However, this setting can still be useful as a showcase for analysis of non-stationary time series and possible directions of future work.

D IMPLEMENTATION DETAILS

All the experiments are implemented in Pytorch [Paszke et al., 2019] and carried out on NVIDIA RTX 2080Ti GPUs.

D.1 ENCODER ARCHITECTURE

Below we provide details of the encoder architectures.

SDCI-Static encoder The first design of the architecture extends directly from ACD [Löwe et al., 2020] and we refer to this model as SDCI-Static. We discuss the network construction for hidden state case as an example, for which the logits $\boldsymbol{\phi}_{ij}$ for the distribution $q_\phi(\mathbf{W}|\mathbf{X})$ are obtained as follows. First, the model computes a latent embedding for each node i using the whole sequence:

$$\mathbf{h}_i^1 = f_{\phi_1}(\mathbf{x}_i^{1:T}). \tag{22}$$

Then each embedding is updated using a graph neural network (GNN) that captures the correlations between nodes. Specifically the message passing procedure follows the two equations below:

$$\mathbf{h}_{ij}^1 = f_{\phi_2}(\mathbf{h}_i^1, \mathbf{h}_j^1), \tag{23}$$

$$\mathbf{h}_i^2 = f_{\phi_3}\Big(\sum_{i \neq j} \mathbf{h}_{ij}^1\Big). \tag{24}$$

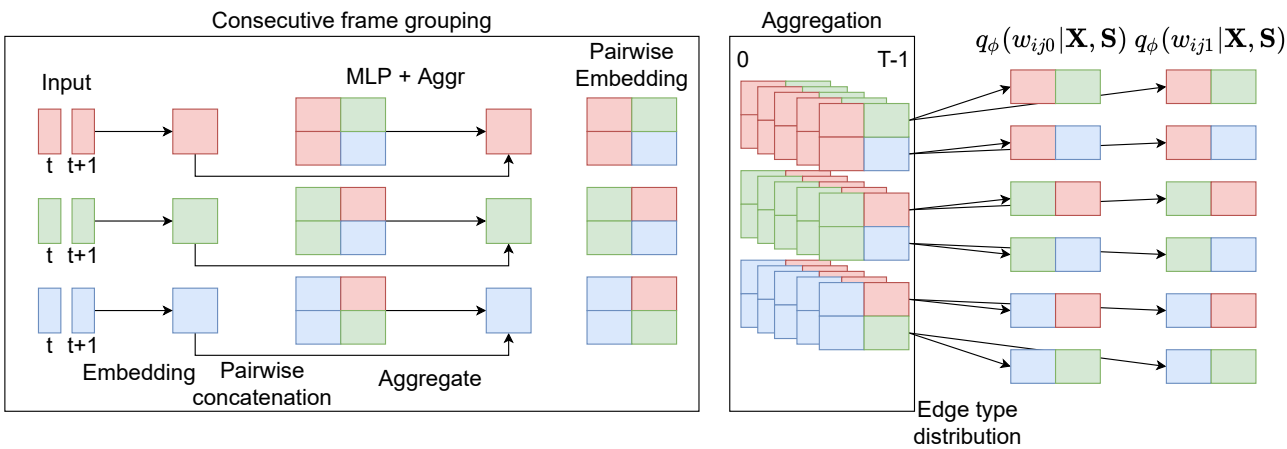

Figure 7: Illustration of the implementation of the SDCI-Temporal encoder, which preserves the local temporal information and aggregate it at last. In the example, we consider 2 states.

Finally, we obtain the softmax logit $\boldsymbol{\phi}_{ij} \in \mathbb{R}^{K \times n_\epsilon}$ for every possible edge $\mathbf{x}_i \to \mathbf{x}_j$ and every possible state $1 \leq k \leq K$:

$$\boldsymbol{\phi}_{ij} = f_{\phi_4}(\mathbf{h}_i^2, \mathbf{h}_j^2). \tag{25}$$

The above network architecture design is visualised in Figure 6. according to equation 6. The details of the architecture settings follows the design in Löwe et al. [2020]. Each embedding step f_{ϕ_i} uses two-layers of 256 dimensions and ELU [Clevert et al., 2016] activations followed by a batch normalization. f_{ϕ_4} uses skip connections and we modify its output size to generate a pairwise embedding for each of the K states. For fully-observed state case, the architecture for $q_\phi(\mathbf{W}|\mathbf{X}, \mathbf{S})$ follows a similar structure, except that for the first layer we use $\mathbf{h}_i^1 = f_{\phi_1}(\text{concat}(\mathbf{x}_i^{1:T}, \mathbf{s}_i^{1:T}))$, where $\mathbf{s}_i^{1:T}$ is a set of one-hot vectors representing the states $\{s_i^t\}_{t=1}^T$.

SDCI-Temporal encoder To preserve the temporal ordering information in the encoder, we propose another encoder design, named SDCI-Temporal, which pays attention to capturing the first-order dynamical structure in the data. Again using the hidden state case as an example, the encoder transformations are defined as:

$$\mathbf{h}_i^{1,t} = f_{\phi_1}(\mathbf{x}_i^t, \mathbf{x}_i^{t+1}), \tag{26}$$

$$\mathbf{h}_{ij}^{1,t} = f_{\phi_2}(\mathbf{h}_i^{1,t}, \mathbf{h}_j^{1,t}), \tag{27}$$

$$\mathbf{h}_i^{2,t} = f_{\phi_3}\Big(\sum_{i \neq j} \mathbf{h}_{ij}^{1,t}\Big), \tag{28}$$

$$\mathbf{h}_{ij}^{2,t} = f_{\phi_4}(\mathbf{h}_i^{2,t}, \mathbf{h}_j^{2,t}), \tag{29}$$

$$\boldsymbol{\phi}_{ij} = f_{\phi_{aggr}}(\{\mathbf{h}_{ij}^{2,t}\}_{t=1}^{T-1}) \tag{30}$$

Figure 7 shows the structure of the SDCI-Temporal encoder. We no longer use the whole sequence at first, but concatenate consecutive frames and set it as the input to f_{ϕ_1}, we perform this computation from 1 to $T-1$ time-steps. In the case of fully observed states, $\mathbf{x}_i^t$ and $\mathbf{x}_i^{t+1}$ are replaced by $\text{concat}(\mathbf{x}_i^t, \text{one-hot}(s_i^t))$ and $\text{concat}(\mathbf{x}_i^{t+1}, \text{one-hot}(s_i^{t+1}))$ respectively as the inputs to f_{ϕ_1}. All the subsequent steps, except for the aggregator $f_{\phi_{aggr}}$ have the same structure as the SDCI-Static encoder.

The design of the aggregator $f_{\phi_{aggr}}$, which aims to summarize the temporal correlations captured throughout the whole sequence, is crucial to the performance of SDCI-Temporal encoder. Preliminary empirical results showed that with an MLP $f_{\phi_{aggr}}$, SDCI-Temporal performs poorly for inferring causal structures from data. Instead we proposed a 1D CNN for aggregation, which reported better results. In detail, for the main text experiments, $f_{\phi_{aggr}}$ consists of two-layer 1D CNN of 256 filters of window size 5 plus a maxpool operation for the final aggregation. Future work towards designing better aggregation schemes might consider attentive pooling [Lin et al., 2017], or simply perform an average pool.

D.2 TRAINING SPECIFICATIONS

All the models participating in the experiments of this section have been trained using the following training scheme, including ACD [Löwe et al., 2020].

Customized decoder (linear data only) One of our objectives in the linear data experiments is to recover the underlying world parameters $\{\beta_k\}_{k=1}^{n_\epsilon - 1}$. Therefore the decoder design imitates the message passing operation presented in Eq. 31, which allows us to initialize the decoder using the underlying world parameters and analyse the performance of the encoder as a separate entity from the whole model.

Hyper-parameters Following Kipf et al. [2018], the models are trained using ADAM optimizer [Kingma and Ba,

2015]. The learning rate of the encoder is $5 \cdot 10^{-4}$, the learning rate of the decoder is $1 \cdot 10^{-3}$ for the synthetic linear data experiments and $5 \cdot 10^{-4}$ for spring data experiments. Learning rate decay is in use with factor of 0.5 every 200 epochs. We train for 1000 epochs in the linear experiments and 500 epochs in the springs experiments, using a batch size of 128. The decoder is trained with teacher forcing every 10 time-steps, i.e., it receives the ground-truth as input every 10 time-steps. The temperature τ is set to 0.5 and the variance of the Gaussian distribution of the decoder is $\sigma^2 = 5 \cdot 10^{-5}$. When considering the setting where we make the state dependent on the dynamics of the objects (scenarios 2 and 3), we set $\lambda = 10^3$. For inferring the hidden states, we set the temperature $\gamma = 0.1$ in the linear experiments and $\gamma = 0.05$ in the spring data experiments.

E EVALUATION

E.1 SUMMARY GRAPH IN TDFCM

Huang et al. [2015] do not specify explicitly the computation of the summary graph (or an equivalent object). To allow a fair comparison, we take the same approach as in Huang et al. [2019], where and edge from i to j is not incorporated in the summary graph if the corresponding estimated time-varying coefficient has mean and variance lower than a theshold.

E.2 ACCURACY OF THE SUMMARY GRAPH

To clarify, the evaluation of the summary graph considers correctly classifying the interaction between all pairs of nodes in both directions. To exemplify, see Figure 5b. In this case, we have N=3 variables, which means that our method needs to produce 6 predictions (one for every pair of edges in both directions). We then compute the accuracy of these predictions and average across all the samples in the test set.

E.3 COMPUTING THE SUMMARY GRAPH IN SDCI

Notice that SDCI can extract the conditional summary graph (CSG) whereas the baselines we compare with only consider the summary graph (SG). Consequently, the only immediate way to compare the performance in capturing the causal structure among the methods we consider is to evaluate the latter. From the definition of summary graph, we deduce that one can estimate it by taking the union of the graphs in the CSG. This is used to compute the summary graphs of both SDCI and the ground truth structure of the generative process.

F DATASETS

In this section we provide detailed information about the datasets used in this work. We generate 50000 samples of each setting for training the models. Regarding testing, we compute all the metrics using 10000 samples, except when comparing with CD-NOD and SAEM, where we use 200 samples since they require retraining the whole model for each sample. However, notice that for both baselines we use sequences of much longer length (e.g., $T = 100$ or $T = 1000$) as these methods rely on longer sequences to get accurate results.

F.1 LINEAR DATA

The ground-truth structural equation for the data generation process at time t is

$$\mathbf{x}_j^{t+1} = \alpha \mathbf{x}_j^t + \sum_{i \neq j}^{N} \beta_k \mathbf{x}_i^t + \boldsymbol{\epsilon}_j^t, \quad k = \left(\mathcal{E}_{s_i^t}\right)_{ij}, \tag{31}$$

where $\alpha \in \mathbb{R}$ controls the self-connection, and $\boldsymbol{\epsilon}_i^t$ denotes independent noise sampled at each time-step.

Below we provide details of the data generation process for the linear data. First, we set the edge-type interactions. In our experiments we set $\alpha = 0.9$, $\beta_1 = 0.5$, and $\beta_2 = -0.5$ and $\boldsymbol{\epsilon}_i^t \sim \mathcal{U}(-0.2, 0.2)$. To generate each sample, we need to sample the initial values of the continuous variable for each element, $\mathbf{x}_i^0 \sim \mathcal{N}(0, 2)$, and the underlying causal structure dependent on the state, $\mathcal{G}_{1:K}$. At each time-step, it suffices to query the edge-type k for each pair of variables and apply the corresponding causal effect β_k following Equation 31. The edge-type is $k = \left(\mathcal{E}_{s_j^t}\right)_{ji}$, where $(\mathcal{E}_s)_{ji}$ denotes the causal effect from j to i at state s, which has been defined at the beginning of the sequence. For all our experiments with this dataset, we simulate $N = 3$ variables. When considering hidden states in scenario class 2, we set $s_i^t = \mathbf{1}_{(|\mathbf{x}_i^t| > 2)}$ (2 states).

There are potential concerns that the generated samples produced in the linear data may be unstable. Still we use this data for one of the evaluations with the following reasons. First, they define a simulated environment where one has the ground truth and can debug and control simulation errors with ease. Furthermore, for one-dimensional variables $\mathbf{x}_i \in \mathbb{R}$ (which is our case), this dataset reduces to a first order Vector Autoregressive (VAR) model [Sims, 1980], which is widely used in works related to causal discovery for time series data [Gong et al., 2015]. The evolution of a sequence in this case can be expressed as follows:

$$\mathbf{x}^t = \mathbf{A}\mathbf{x}^{t-1} + \mathbf{e}^t \tag{32}$$

where $\mathbf{A}$ is the causal transition matrix and $\mathbf{e}^t$ is an independent noise process.

Regarding stability, the samples in this dataset are described by a causal transition matrix $\mathbf{A}$ where the diagonal elements are α and the off-diagonal elements are β_k where k is the edge-type interaction. For a first-order VAR to be stable, the singular values of $\mathbf{A}$ need to be smaller than one. Taking into the account that each sample can obey a different underlying causal graph, one needs to check this condition for all the possible arrangements of the off-diagonal elements (since the diagonal elements are always α). The number of matrices that one needs to check grows rapidly for increasing number of variables, which makes the verification of this condition computationally infeasible (recall that computing the eigenvalues of a matrix has cubic cost $O(N^3)$). In practice, we generate random samples and keep them if the magnitude of the last observation is comparable to the initial one. We also require that the states are visited in similar proportions to satisfy our assumptions on the data.

F.2 SPRING DATA

When considering springs with directed connections, we follow the generation procedure described Kipf et al. [2018] with a small modification where the spring interaction between a pair of particles can change over time (depending on the state).

In this dataset, N particles are simulated inside a 2D box where they can collide elastically with its walls. Each pair of variables is connected by a spring with uniform probability. To allow for identification of causal connections (directed edges), the connection is made unidirectional. The springs interact via the Hooke's law and this setting yield the following equations:

$$\mathbf{f}_{ij} = -\delta_k(\mathbf{r}_i - \mathbf{r}_j), \quad \ddot{\mathbf{r}}_i = \sum_{j=1}^{N} \mathbf{f}_{ij}, \quad \mathbf{x}_i = \{\mathbf{r}_i, \dot{\mathbf{r}}_i\} \quad (33)$$

where $\mathbf{f}_{ij}$ is the unidirectional interaction from particle j to particle i, δ_k denotes the edge-type for each pair of variables, and $\mathbf{r}_i$ and $\dot{\mathbf{r}}_i$ denote the 2D position and velocity of each particle. The continuous variable $\mathbf{x}_i$ is constructed by concatenating the position and the velocity measurements.

Notice that the above equation defines the evolution of the continuous variable for a single time-step. In our setting, we have that $k = \left(\mathcal{E}_{s_j^t}\right)_{ji}$. Thus, $\mathbf{f}_{ij}$ will change over time, contrary to Kipf et al. [2018]. Since we consider two edge-types, we define $\delta_0 = 0$ and $\delta_1 = 0.1$. To generate samples, we first generate a random conditional summary graph $\mathcal{G}_{1:K}$ and the initial location and velocity. Then, trajectories are simulated by solving the previous differential equations using leapfrog integration. The step size used is 0.001 and the trajectories are obtained by sub-sampling each 100 steps. In our experiments, we set $N = 5$ and $T = 80$. When considering hidden states in scenario class 2, we set $s_i^t = \mathbf{1}_{(\mathbf{x}_i^t > 0)}$ (2 states).

Table 3: Test edge-type accuracy (in %) and MSE for linear data generated with scenario class 1 settings.

METHOD	EDGE ACCURACY	TEST MSE
ACD - FIXED DECODER	66.02 ± 0.29	$0.49 \pm 1.89 \cdot 10^{-2}$
ACD	66.44 ± 0.29	$0.47 \pm 1.98 \cdot 10^{-2}$
SDCI - STATIC - FIXED DEC.	90.43 ± 0.23	$2.64 \cdot 10^{-2} \pm 4.55 \cdot 10^{-3}$
SDCI - STATIC	93.84 ± 0.19	$1.57 \cdot 10^{-2} \pm 4.03 \cdot 10^{-3}$

G ADDITIONAL RESULTS

In this section we report additional experiments and qualitative visualisations, which can be helpful to complement the main results from Section 4 in the main text.

G.1 LINEAR DATA

Results for scenario class 1 We consider the case of scenario class 1 (see Section 1) where the states $\mathbf{S}$ are observed and their dynamics are independent from $\mathbf{X}$. We compare SCDI-Static with ACD, and evaluate the effect of explicitly modeling the underlying state. We further consider the case where the decoder is fixed and uses the ground-truth β_k values, for which we denote as - FIXED DECODER or - FIXED DEC. for short.

Table 3 shows the edge-type identification accuracy and test data reconstruction mean-squared error (MSE) for a simulation with $N = 3$ variables, $K = 2$ states, and $n_\epsilon = 2$ edge-types (no-edge and β_1). SDCI-Static successfully performs the task of identifying the edges. In terms of the ℓ_1 error for estimating $\{\beta_k\}$, ACD scores worse ($\sim 10^{-3}$) compared to SDCI ($\sim 10^{-5}$).

We also evaluate SDCI-Temporal on the synthetic linear data with 2 edge-types and 2 states. Table 4 extends the results reported in Table 3 in the main text. We see that SDCI-Temporal models generally return worse results than SDCI-Static models. Specifically, SDCI-Temporal performs much worse when using learned decoder, and it fails to identify the underlying causal structure thus producing inaccruate forecasting results (see test MSE). Further inspection also shows that its ℓ_1 error for estimating $\{\beta_k\}$ is considerably higher ($\sim 10^{-2}$) than ACD and SDCI ($\sim 10^{-3}$ and $\sim 10^{-5}$ respectively). Given that SDCI-Static with learned decoder returns accurate results, the failure of SDCI-Temporal is attributed to the inaccurate posterior approximation in VAE learning, which justifies improvement need for the aggregator $f_{\phi_{aggr}}$ as already discussed in Appendix D.1.

We repeat the same experiments with 3 edge-types and 2 states, and report the results in Table 5. As before, SCDI-Static shows superior performance in comparison to ACD and SCDI-Temporal. Notice that the latter achieves similar accuracy scores in comparison to its FIXED DECODER setting. In terms of the ℓ_1 error for estimating $\{\beta_k\}$, we observe that both SDCI-Static and SDCI-Temporal provide more accurate estimations ($\sim 10^{-2}$ and $\sim 10^{-3}$ respec-

Table 4: Test edge-type accuracy (in %) and MSE for linear data generated with scenario class 1 settings (fully-observed states) for 2 states and 2 edge-types.

METHOD	EDGE ACCURACY	TEST MSE
ACD - FIXED DECODER	66.02 ± 0.29	$0.49 \pm 1.89 \cdot 10^{-2}$
ACD	66.44 ± 0.29	$0.47 \pm 1.98 \cdot 10^{-2}$
SDCI - STATIC - FIXED DEC.	90.43 ± 0.23	$2.64 \cdot 10^{-2} \pm 4.55 \cdot 10^{-3}$
SDCI - STATIC	93.84 ± 0.19	$1.57 \cdot 10^{-2} \pm 4.03 \cdot 10^{-3}$
SDCI - TEMPORAL - FIXED DEC.	82.79 ± 0.28	$7.43 \cdot 10^{-2} \pm 4.79 \cdot 10^{-3}$
SDCI - TEMPORAL	49.97 ± 0.28	$0.84 \pm 3.29 \cdot 10^{-2}$

Table 5: Test edge-type accuracy (in %) and MSE for linear data generated with scenario class 1 settings (fully-observed states) for 2 states and 3 edge-types.

METHOD	EDGE ACCURACY	TEST MSE
ACD - FIXED DECODER	49.29 ± 0.31	$0.50 \pm 1.56 \cdot 10^{-2}$
ACD	34.11 ± 0.28	$0.66 \pm 2.52 \cdot 10^{-2}$
SDCI - STATIC - FIXED DEC.	92.75 ± 0.22	$1.00 \cdot 10^{-2} \pm 1.57 \cdot 10^{-3}$
SDCI - STATIC	84.36 ± 0.28	$3.64 \cdot 10^{-2} \pm 2.19 \cdot 10^{-3}$
SDCI - TEMPORAL - FIXED DEC.	70.99 ± 0.31	$9.95 \cdot 10^{-2} \pm 4.45 \cdot 10^{-3}$
SDCI - TEMPORAL	72.28 ± 0.31	$9.64 \cdot 10^{-2} \pm 3.64 \cdot 10^{-3}$

tively) compared to ACD ($\sim 10^{-1}$). Compared to the failure of SDCI-Temporal (learned decoder) in the previous experiment, one can deduce that accurate estimation of the edge-type parameters plays a crucial role in learning to infer the underlying causal structure. This is further illustrated in Figure 8 which shows the evaluation metric curves of SDCI-Temporal during training. Here the edge-type accuracy improves when the $\{\beta_k\}$ are estimated correctly, in which the l_1 estimation error tends towards zero.

Scenario class 2 The results considering linear data with hidden states in scenario class 2 show that the CSG accuracy decreases when considering an additional edge-type (see Table 1). However, when leaving the summary graph constant (3-EDGE CONST) we obtain better CSG estimations. Figure 9 shows the approximate posterior $q_\phi(s_i^t|\mathbf{x}_i^t)$ inferred by SDCI-Static in each of the 3 settings studied in this experiment along with the true underlying state function, $s_i^t = \mathbf{1}_{(|\mathbf{x}_i^t|>2)}$. We notice that SDCI-Static achieves better results when the quality of the estimated state function is

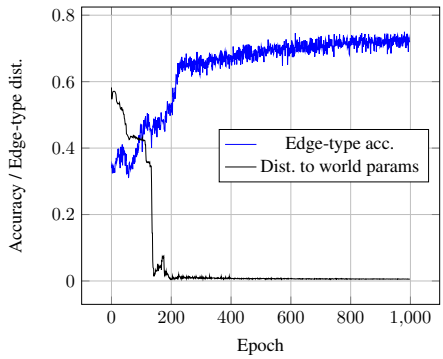

Figure 8: Edge type accuracy and l_1 error for estimating $\{\beta_k\}$ for SDCI-Temporal as a function of training epoch for 3 edge-types in scenario class 1.

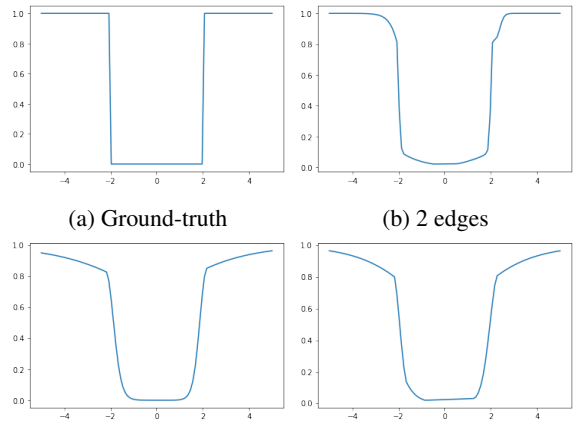

(a) Ground-truth (b) 2 edges

(c) 3-edges const (d) 3-edges free

Figure 9: Underlying state function for scenario class 2 in the linear dataset, $s_i^t = \mathbf{1}$.

Table 6: Test Edge-type accuracy (in %) and test MSE using spring data with state transitions on wall collision.

METHOD	EDGE ACCURACY	TEST MSE	STATE ACC
ACD	68.63 ± 0.14	$1.46 \cdot 10^{-3} \pm 1.35 \cdot 10^{-5}$	98.21 ± 0.02
SDCI-STATIC	79.19 ± 0.14	$1.39 \cdot 10^{-3} \pm 1.33 \cdot 10^{-5}$	98.53 ± 0.02

higher. This is expected, since querying the correct edge-type from the conditional summary graph strongly relies on accurate state estimations. Therefore, the model has to learn the state distribution and only then will be able to infer accurate causal structures. Although they can be challenging in general, our results show that SDCI-Static is successful in performing both learning steps in simple settings. This offers a promising direction of work towards the conditional stationary setting with hidden states.

Figure 10 shows samples for the linear data considering hidden states and 2 edge-types along with the corresponding causal summary graphs and summary graphs inferred by both SDCI-Static and ACD. Since SDCI-Static achieves high accuracy, the majority of the graph estimations match the true causal summary graph, which results in good forecasts. We also show two cases (two last rows) where the graph estimations do not match the ground-truth, and in these cases the model does not predict the future trajectories accurately. Similar to what we show in the main text, the trajectories obtained with ACD drop rapidly to 0, and the summary graph estimates are considerably worse.

G.2 SPRINGS DATA

Scenario class 3 We consider the case where the particles are contained in a box, and the state of a particle transitions when it collides with the wall of the box (see Figure 1c). For simplicity, we only consider $K = 2$ states that transition alternatively on wall collision. We report SDCI's performance along with ACD in Table 6. Regarding edge accuracy SDCI

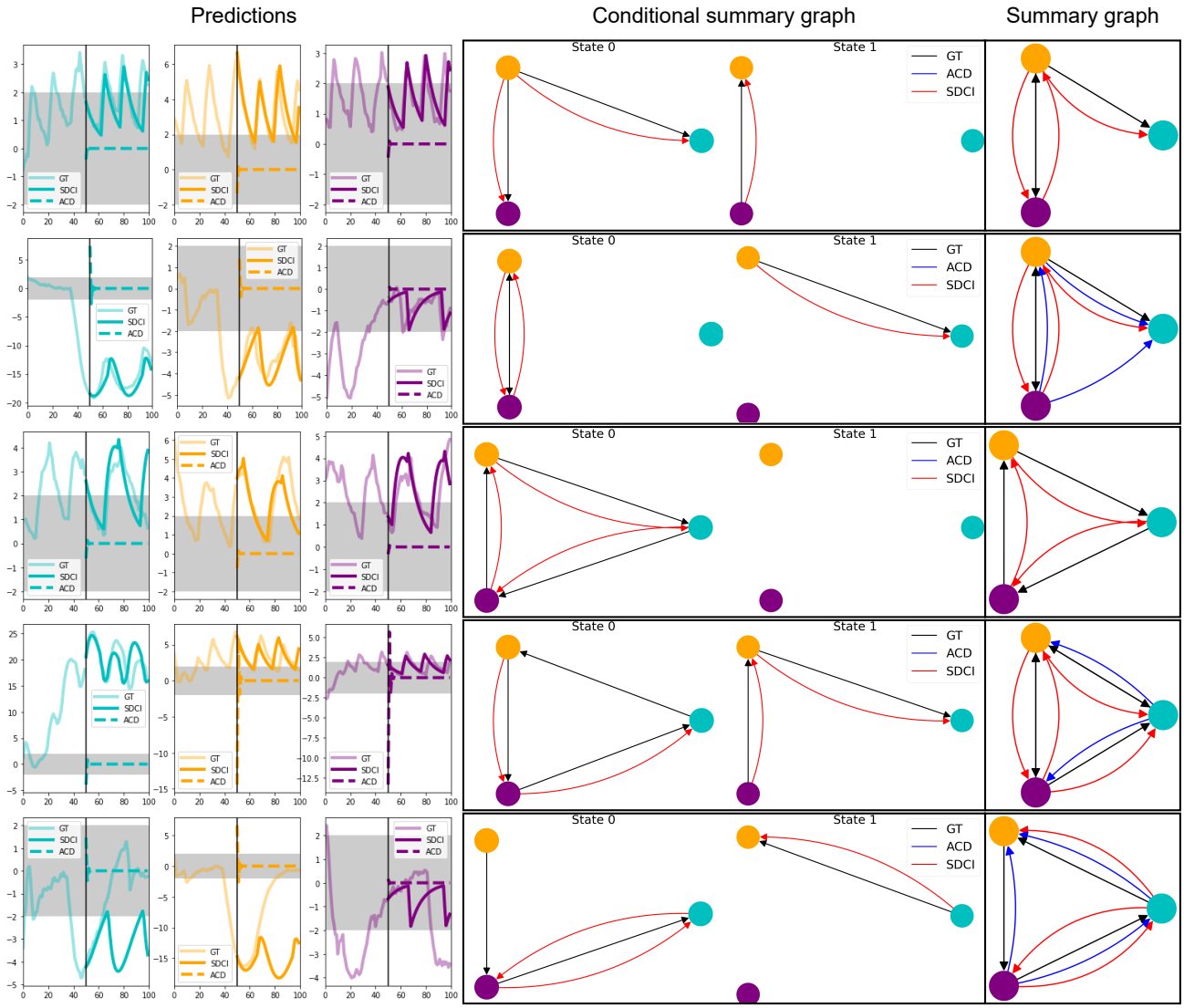

Figure 10: time series forecasting (left) of both SDCI (solid line) and ACD (dashed line) for 50 time-steps along with the ground-truth (GT, transparent line). The first 50 time-steps are given to the models as input and the background color represents the state value. We show the associated conditional summary graph (center) and summary graph (right) of SCDI (red) and ACD (blue) along with the ground-truth (GT, black) for each sample. Each row represents a different sample.

Table 7: Summary graph (SG) and conditional summary graph (CSG) accuracies of the different causal discovery methods considering hidden states in the springs dataset.

METHOD	SG ACCURACY	CSG ACCURACY
CD-NOD (T=160)	30.05 ± 1.42	-
CD-NOD (T=1000)	35.53 ± 1.37	-
ACD (T=80)	67.19 ± 1.52	-
SDCI-STATIC (T=80)	77.95 ± 1.08	80.93 ± 1.33

performs significantly better, and ACD is limited by considering stationary dynamics only. However, both methods achieve comparable test MSE metrics, indicating that that ACD can still make decent predictions even when it fails in identifying the edge-type interactions.

Scenario class 2 (hidden) We provide additional visualisations for the case with hidden states in Figure 11, where we show the predictions of both SDCI-Static and ACD as well as the corresponding conditional summary graphs and summary graphs extracted by both methods respectively. As in the linear case, SDCI-Static produces accurate causal graph estimates. Regarding time series forecasting, our method is able make reasonable predictions. Notice that to train the models, we use teacher forcing every 10 time-steps, which means that the learned models are less suited for long-term dynamics modelling. However, one can expect to obtain more accurate predictions by progressively reducing the teacher forcing frequency during training. Considering ACD, despite being restricted by assuming stationary time series, it still infers graph structures that allow the model to produce decent forecasts.

Results for scenario class 2 We consider the hidden state regime, where the underlying state of a particle changes depending on its location in the box ($K = 2$, see Figure 1b). Results in Table 7 shows a clear advantage of SDCI over baselines in terms of summary graph identification accuracy, and its accuracy levels are closer to the levels in scenario class 3 with observed states (table 6). Again ACD is limited by its stationary dynamics assumption, and CD-NOD fails due to its inability in handling discrete changes in the causal effects of the full time graph.

We visualize the time series forecasting results (for 50 time-steps) with SDCI and ACD given an input sequence of $T = 80$ time-steps in Figure 12, as well as the extracted & ground truth (conditional) summary graphs in Figure 13. We see that the conditional stationarity assumption of SDCI allows it to extract more accurate graph structures, which result in better predictions in comparison to ACD.

Overall, our method successfully decomposes the non-stationary dynamics into the conditional stationary ones while capturing the state transition dynamics.

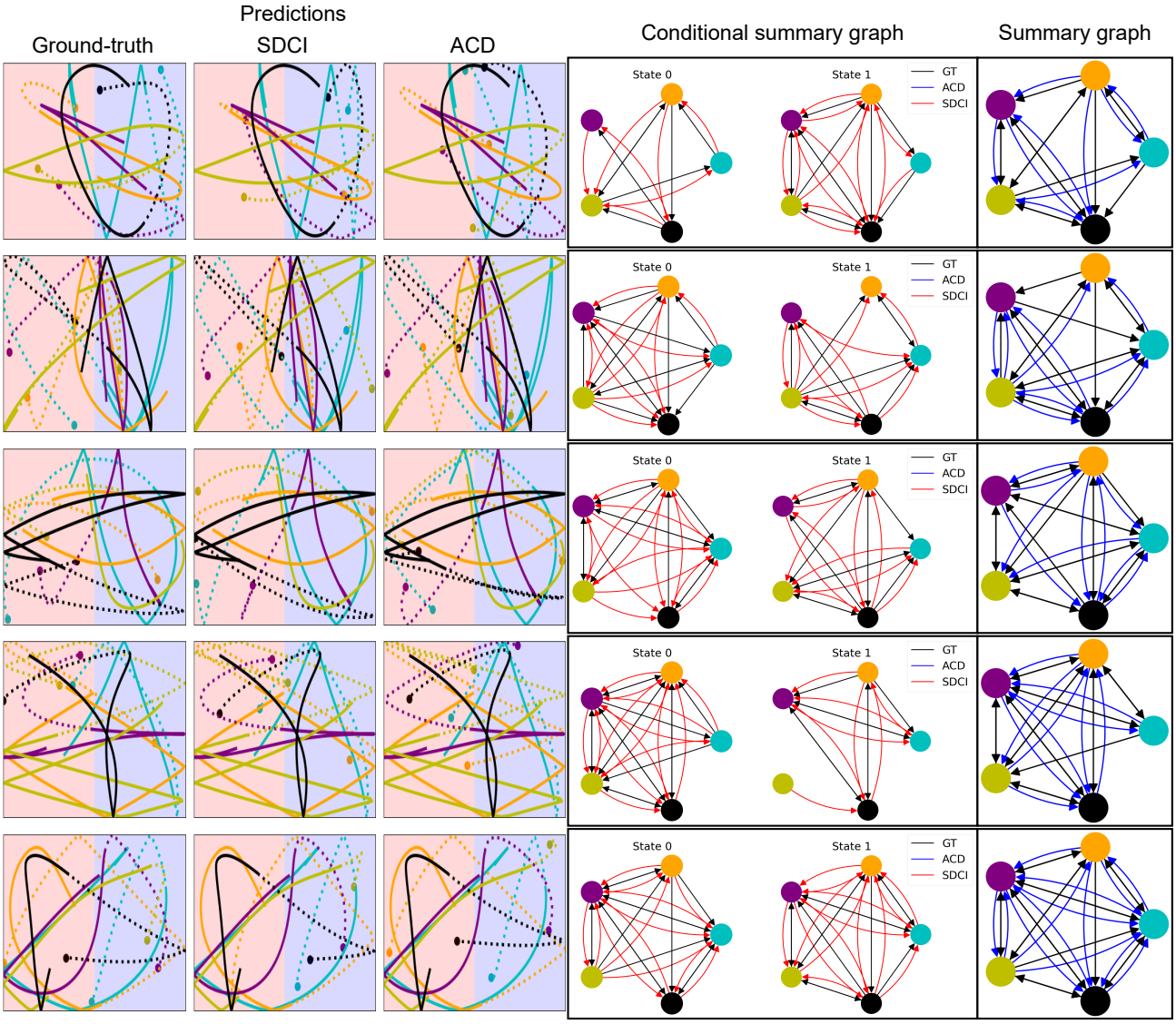

Figure 11: time series forecasting (left, dotted lines) of SDCI and ACD for 50 time-steps along with the ground-truth. We use solid lines to denote the input to the models and the background color represents the state value. We show the associated conditional summary graph (center) and summary graph (right) of SCDI (red) and ACD (blue) respectively along with the ground-truth (GT, black) for each sample. Each row represents a different sample.

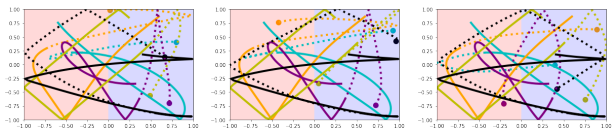

(a) ground-truth (b) SDCI (c) ACD

Figure 12: time series forecasting (dotted lines) of both (b) SCDI and (c) ACD for 50 time-steps along with (a) the ground-truth. The trajectories in solid lines are used as the input and the background color represents the state value.

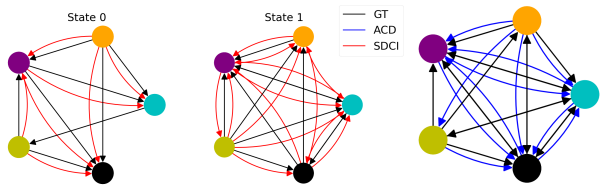

(a) (b)

Figure 13: (a) Conditional summary graph and (b) summary graph of SCDI (red) and ACD (blue) respectively, along with the ground-truth (black).